Biogeochemistry (2011) 103:159–180
DOI 10.1007/s10533-010-9454-1

Porewater nitrate profiles in sandy sediments hosting submarine groundwater discharge described by an advection–dispersion-reaction model

J. Severino P. Ibánhez · Catarina Leote · Carlos Rocha

Received: 15 April 2009 / Accepted: 15 April 2010 / Published online: 18 May 2010

Abstract In order to separate the effects of reaction from those of transport on vertical porewater concentration profiles of nitrate at an intertidal groundwater seepage site (Ria Formosa, Portugal), a free-boundary solution of an Advection–Dispersion-Reaction (ADR) model was used to describe the shape of NO_3^- concentration profiles collected in situ. The model includes three sequential reaction layers, postulated with basis on the local distribution of the benthic organic C:N ratio and major identifiable changes in concentration gradients with depth. The advective nature of the system was used to propose a mass balance simplification to the constitutive equations permitting a free-boundary solution, which in turn allowed prediction of sediment–water fluxes of NO_3^-. Sensitivity analysis confirmed that in similarly advective-dominated environments, both the porewater concentration distribution and the interfacial fluxes are strongly dependant on seepage rate and benthic reactivity. The model fitted the measured profiles with high correlation (usually higher than 90%), and model-derived sediment–water NO_3^- fluxes were in good agreement to fluxes measured in situ with Lee-type seepage meters (0.9948 slope, $R^2 = 0.8672$, $n = 8$). Nitrate oxidation and reduction rates extracted from model fits to the data (10^{-2}–10^0 mmol m^{-2} h^{-1}) agreed with literature values. Because dispersive effects are not included in direct mass balances based on the porewater concentrations, the model presented here increases the accuracy of apparent reaction rate estimates and geochemical zonation at Submarine Groundwater Discharge (SGD) sites. The results establish the importance of sandy sediments as reactive interfaces, able to modulate mass transfer of continental-derived contaminants into coastal ecosystems. We suggest that tools such as the one described here might be used to advantage in preparing further experimental studies to elucidate how benthic reactivity affects nitrate distribution and fluxes in sediments affected by SGD.

Keywords Beach · Diagenesis · Discharge · Groundwater · Nitrate · Modeling · Sand · SGD

J. S. P. Ibánhez (✉) · C. Rocha
School of Natural Sciences, Trinity College, Dublin, Ireland
e-mail: pinoibaj@tcd.ie

C. Rocha
e-mail: rochac@tcd.ie

C. Leote
Department of Marine Chemistry and Geology, Royal Netherlands Institute for Sea Research (Royal NIOZ), Texel, The Netherlands
e-mail: Catarina.Leote@nioz.nl

List of symbols

z	Depth (L)
$\hat{C}(z)$	Concentration of solute per sediment volume (M L^{-3})

C_0	Concentration of solute per sed. vol. at the upper interface (M L^{-3})
C_{aq}	Concentration of solute per sed. vol. at the lower interface (M L^{-3})
D_{molec}	Molecular diffusion in water (L^2 T^{-1})
D_{if}	Molecular diffusion in sediment (L^2 T^{-1})
D_{isp}	Mechanical dispersion (L^2 T^{-1})
D_{ef}	Efective dispersion (L^2 T^{-1})
v	Advective velocity (L T^{-1})
K_n	Nitrification rate (M L^{-3} T^{-1})
K_d	Nitrate reduction rate (T^{-1})
L_x	Layer depth limit (L)
P_e	Peclet number
D_{a1}	Damköhler number for nitrification
D_{a2}	Damköhler number for nitrate reduction
J	Flux per area of total sediment (M L^{-2} T^{-1})
φ	Porosity
θ	Tortuosity

Introduction

Human activities now fix more atmospheric N into the global Nitrogen cycle than the remainder of Earth's ecosystems (Vitousek et al. 1997). Hence, natural systems have become artificially enriched in N species, while coastal waters became a common depository for this new available N (Mackenzie et al. 2002). Consequences of this progressive increase in Nitrogen loading of coastal systems include local eutrophication, leading to loss of water quality and biodiversity (Herbert 1999; Rabouille et al. 2001).

Although riverine and point-source transport of nutrients have received much attention as pathways for the transport of excess N from land to sea, the role of other routes such as underground flow paths leading to coastal zone N loading have only been recognized recently (Moore 1999; Burnett et al. 2003). This knowledge gap is explained in part by the difficulty of identifying and directly measuring the discharge, because of its spatial and temporal variability (Nowicki and Portnoy 1999; Burnett et al. 2006; Taniguchi et al. 2006; Bowen et al. 2007). Based on similarities with estuarine mixing zones, Moore (1999) established the "subterranean estuary" concept applied to the mixing zone between seawater and groundwater. This concept is intertwined with the Submarine Groundwater Discharge (SGD) phenomenon, which refers to the discharge itself, defined as "any and all flow of water on continental margins from the seabed to the coastal ocean, regardless of the fluid composition or driving force" (Burnett et al. 2003).

Total N content of groundwater arriving at the coastal zone, with NO_3^- as the usually dominant form, is highly variable, depending on factors like inland fertilizer application, sewage infiltration, waste landfill and nitrification at the origin (Slomp and Van Cappellen 2004). The subsurface transport and biogeochemical transformation occurring throughout the aquifer sediment, in particular heterotrophic denitrification, recognized so far as the predominant process depleting groundwater N, can also modulate the final NO_3^- concentration arriving at coastal seepage areas (Bowen et al. 2007; Rivett et al. 2008). However, heterotrophic denitrification is heavily dependant on electron-donor availability, and the lack of labile organic matter could be responsible for the usually high concentrations of oxidized nitrogen arriving at the seepage areas (Slomp and Van Cappellen 2004; Kroeger and Charette 2008; Rivett et al. 2008). Consequently, nitrate attenuation at the sea water-groundwater mixing zone could strongly depend on the amount and quality of electron donors fed from the surface, thus affecting the resulting NO_3^- seepage fluxes (Bowen et al. 2007).

The classical biogeochemical paradigm of sediment accumulation and diffusion-limited reaction has neglected the role of sands on energy and material cycling in coastal sediment beds (Boudreau et al. 2001; Rocha 2008). Low standing stocks of organic matter and mineralization by-products were used to justify this misconception. However, sandy sediments in general and those affected by SGD in particular have recently come under scrutiny as zones of important biogeochemical transformation (Ueda et al. 2003; Slomp and Van Cappellen 2004; Bowen et al. 2007; Kroeger and Charette 2008). Advective motion, characteristic of permeable sediments, enhances the difficulty discriminating between relative roles of transport and reaction processes affecting benthic porewater solute concentrations (Boudreau et al. 2001; Rocha 2008). Moreover, permeability of sands could enhance benthic reaction rates (e.g., Huettel et al. 1998; Falter and Sansone 2000). Thus, the classical approaches to study the biogeochemistry of sediments based on diffusion-limited solute transport are invalid in sandy environments: field sampling needs to preclude

interference with the porewater flow patterns (Seeberg-Elverfeldt et al. 2005), and fluxes and reaction rates cannot be accurately estimated from porewater chemical gradients based on Diffusion–Reaction models (Boudreau 1997; Roychoudhury 2001). Furthermore, mechanical dispersion, caused by transport of a solute through a spatially varying flow field coupled with molecular diffusion, could cause flawed direct mass balances if not considered: solute gradients cannot be directly or exclusively linked to benthic reactivity with significant dispersion in place (Roychoudhury 2001; Bijeljic and Blunt 2006). Within this paradigm, diagenetic modeling could nevertheless be an important tool to understand the biogeochemical role of sandy sediments at seepage sites (see Berner 1980; Boudreau 1997). Advection–diffusion and ADR modeling were already successfully applied in elucidating surface water-groundwater interactions. Numerical modeling packages MODFLOW and MT3D were extensively used in modeling groundwater flow and interactions in the hyporheic zones (e.g., Lautz and Siegel 2006). In SGD places, Rapaglia and Bokuniewicz (2009) used analytical solutions of the general advection diffusion equation for salt to quantify dispersive mixing up to 4 m depth. Moreover, Spiteri et al. (2008) used a numerical 2-D ADR model to quantify main diagenetic processes in SGD faces up to 8 m depth. Nevertheless, strong diagenetic modulation of solute loads are likely to occur within the first few centimeters depth of SGD seepage faces (Rocha et al. 2009). Labile organic matter distribution can be restricted to the top cm (Rocha et al. 2009) and thus can control the behavior of important heterotrophic processes mediating solute loads like denitrification (Slater and Capone 1987; DeSimone and Howes 1996). In this sense, ADR models may be significant tools helping to establish the main reactive zones within the surface benthic concentration gradient, by separating the contribution of advection and dispersion from the role of reaction in changing solute concentrations at different depths. This support may be crucial when sub sampling sediment to carry out laboratory studies using isotope ratios to evaluate reaction kinetics, since criteria underscoring which depths to sub-sample in order to guarantee dominance of a specific nitrogen transforming microbial population would be clearer with the absence of the effect of transport phenomena over substrate concentration profiles.

Here we describe the vertical distribution of NO_3^- concentrations in porewater up to 20 cm depth of sandy intertidal sediments, subject to cyclic, nitrate-rich SGD on the permanently saturated zone with the aid of a mathematical model inclusive of mechanical dispersion. The main objective is to explain and predict the magnitude of observed interfacial fluxes at sediment exposure within an advective-dominated system and suggest preliminary explanations for the extension of different areas of benthic biogeochemical reactivity found in vertical succession at the permanently saturated seepage area.

Methods

Site description and sample collection

The data presented here was collected in the sediment of Praia de Faro (37°00′04″N, 7°88′57″W), one of the two sandy peninsulas of the Ria Formosa coastal lagoon, south Portugal (Fig. 1). Tidal regime in the adjacent coastal area is mesotidal and semidiurnal, with tidal amplitude between 1.35 m in neap tides and 3 m in spring tides (Salles 2001). Tidal regime together with average water column depth in the lagoon (2 m) confer to the Ria a capacity of daily water renewal up to 52–80% of the total volume of the lagoon (Andrade et al. 2004) and simultaneously creates a extensive intertidal zone. The tidal-induced high dilution and mixing capacity along with the relative small freshwater inputs explain the relatively constant salinity of the lagoon (35.5–36.9; Ferreira et al. 2003). Sampling site was selected in the permanently saturated zone within the intertidal area affected by SGD. Large amounts of NO_3^- associated with low salinity water have been documented to seep out during low tide (Leote et al. 2008). Sediment at the sampling site locus of SGD is dominated by medium-coarse sand ($d_p = 0.5$ mm), with high permeability (3.19×10^{-3} cm s^{-1}). Porewater profiles, seepage measurements and sediment cores were taken during two consecutive tidal cycles at spring tides.

Porewater concentration profiles of salinity and NO_3^- were measured monthly from November 2005 to January 2007 by using in situ profilers deployed with poly-ether-sulphone (PES) membranes (Rhizon SMS-10 cm; Eijkelkamp Agrisearch Equipment,

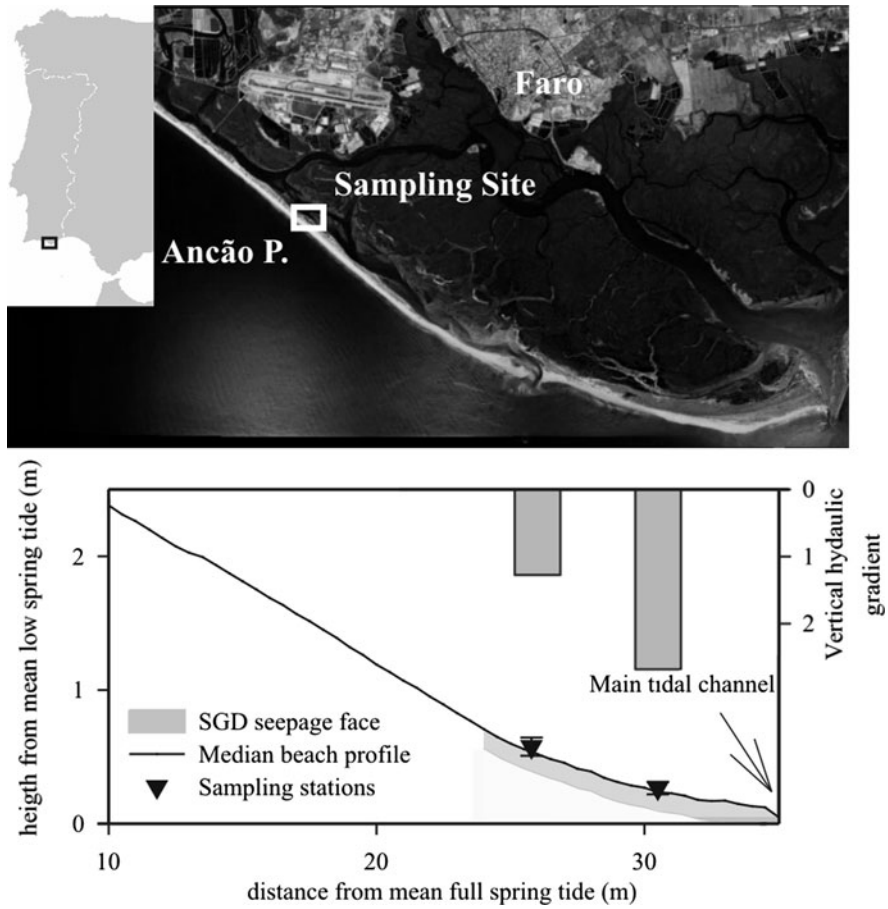

Fig. 1 Sampling site location at the Ria Formosa Coastal Lagoon (South Portugal, image obtained from LandSat). Median beach profile and location of sampling station in the main seepage face as well as relative distance and height related with mean spring low tide are also shown. Bar charts show vertical hydraulic gradient between 40 and 30 cm depth into the sediment measured in April 2006 at low tide

0.1 μm pore size) at constant depths in the sediment. These were mounted on own design in situ acrylic samplers, modified from the design described in Seeberg-Elverfeldt et al. (2005). The samplers were placed along the low-intertidal beach profile and porewater was collected by connecting vacuum tubes to the membranes. The acrylic sampler has the advantage of being left in place throughout the entire experiment causing minimal disturbance to the local benthic flow patterns (Cappuyns et al. 2004; Seeberg-Elverfeldt et al. 2005). The porewater collected this way was ready for analysis without the need of further preservation (Luo et al. 2003; Seeberg-Elverfeldt et al. 2005). Profiles from March and April presented here correspond to the upper limit of the SGD seepage area, since for the other months the porewater profiles were taken within the seepage face, close to the peak discharge (Fig. 1). For direct measurements of advective velocities and fluxes from the sediment, between 2 and 3 Lee-type seepage meters were used at each sampling location, placed in line with the porewater profilers (Fig. 1, Lee 1977; Burnett et al. 2006; Taniguchi et al. 2006). Sampling started one tidal cycle after installation to permit system stabilization. Before sampling started, the two plastic collection bags connected to each seepage meter were left open to fully release any air trapped into the seepage meters or bags. Sampling started during the next sediment exposure phase (ebbing tide) and was carried out during a minimum of two subsequent tidal cycles. During sampling, continuous measurements of seepage velocity, salinity and temperature were performed in the water collection bags connected to the seepage meters, and aliquots were taken for NO_3^- determination. Operation of the seepage meters was performed following the precautions suggested by Cable et al. (1997). Plastic collection bags were kept at the same level as the seepage meters in order to minimize any interference of the bags with the local hydraulic head. Due to

logistic limitations, no pre-determined sampling times were set. Instead, sampling was performed by emptying the content of the bags when they were approximately ¾ full and registering the time of collection. No bag pre-filling was done due to the fast and frequent sampling needed to accomplish our sampling strategy, and to the existence of parallel point piezometers that would either verify the assumption of essentially vertical flow (Fig. 1) or at the very least provide independent gauging of pore pressure allowing comparison. However, as explained in Leote et al. (2008) and further demonstrated in Rocha et al. (2009), this could lead to wrong measurements due to the Shaw-Prepas effect, related to the mechanical properties of the collection bags (Shaw and Prepas 1989). Nevertheless, as also tediously demonstrated by Shaw and Prepas (1989), this artifact is minimal when studying seepage rates higher than 0.5 L h^{-1} m^{-2}. The "Shaw-Prepas" effect should therefore be minimal in our study due to the high recorded seepage rates (lowest recorded rate 0.7 L h^{-1} m^{-2}; Leote et al. 2008). The possible sources of error affecting seepage rate measurements with this technique (i.e., potential alteration of natural hydraulic head when sea water level drops below seepage meters or due to the "Shaw-Prepas" effect) arise uncertainties about our measurements. However, seepage rate records obtained with Lee-type seepage meters at our site showed strong coherence as discussed in Leote et al. (2008) and Rocha et al. (2009). Seepage rates showed strong tidal modulation, with peak rates at sediment exposure concomitant with the lowest salinities. At high tide, minimum or absent seepage rates were measured. Also, seepage rates decreased from the permanently saturated area to the upper levels of the beach. The physical coherence of seepage rate records was further tested by performing independent measurements using sets of mini-piezometers at each seepage meter deployment station (Rocha et al. 2009). Seepage rates were thus calculated from piezometric head in situ by applying Darcy's law. Generally good agreement between seepage meter and piezometer data was confirmed (Rocha et al. 2009). Despite the potential source of error of the seepage meters used, the local use of independent assessment of hydraulic head together with the operation based on literature references (including studies directly evaluating the relative effect of different operational measures, adapted to local conditions), the potential source of error associated with operation of the seepage meters, under these conditions, was effectively minimized.

In order to complement the information obtained with seepage meters and sediment vertical profilers, sediment cores (25 cm length, 3.5 cm diameter) were taken by hand, and sliced on-site for analysis of water content and porosity. Water content was measured in each sub-sample as a percentage of weight loss after freeze-drying for 24 h. Porosity, φ, was calculated by the equation described by Dullien (1992), using 2.65 g mL^{-1} as dry sediment density. Tortuosity, θ, was calculated assuming to obey Archie's law, $\theta^2 = \phi^{1-m}$, where m is a fitting parameter (Boudreau 1997). Experimental fitting work revealed $m = 2$ for sands and mud sediments with porosities lower than 0.7 (Ullman and Aller 1982), thus obtaining the formulation $\theta^2 = \phi^{-1}$ for the tortuosity calculation. Salinity of porewater samples was measured with an ATAGO S/Mill-E hand-held refractometer. Salinity and temperature of the seeped water were determined in situ with an YSI 600 multi-parameter probe (Yellowspring Instruments). NO_3^- content in porewater and seeped water were determined by the spongy cadmium method (Jones 1984). A more complete description of the sampling strategy, methods, and site specifics can be found in Leote et al. (2008).

Modeling approach

Conceptual model

In intertidal sandy sediments affected by SGD, the pressure balance between the hydraulic head of the unconfined aquifer and tide could determine the mass exchange through the sediment–water interface (Johannes 1980). In mesotidal environments, tidal modulation could therefore be the main forcing factor determining water exchange and related solutes across the sediment–water interface (Robinson et al. 2007). Inside the sediment, tide can induce dispersive mixture of both end members (groundwater and sea water) and thus determine the composition of the seeping water (Rapaglia and Bokuniewicz 2009). Moreover, the tide can determine porewater advective velocity due to the changing hydraulic head caused by its rise and fall. Thus, tidal level oscillation can also control the

extent and magnitude of solute mixing within the sediment due to mechanical dispersion (Rapaglia and Bokuniewicz 2009; Roychoudhury 2001). At this site, significant advective velocities were measured in situ, mainly during sediment exposure, when discharge peaked (Leote et al. 2008). The largest fluxes of NO_3^- were associated to groundwater discharge peaks. In effect, tidal dynamics have been identified as the main modulator of temporal patterns of SGD at the Ria Formosa coastal lagoon (Rocha et al. 2009). A cyclic and reproducible discharge pattern was observed, with peak rates at low tide and minimum or absent seepage during peak high tide (Leote et al. 2008, Rocha et al. 2009). Thus, for the purpose of model formulation, advective transport of NO_3^- is assumed to be exclusively the result of the seepage of porewater, accepted as essentially vertical (Fig. 1; Horn 2002; Burnett et al. 2006 and references therein). In fact, the possible horizontal component of seepage can introduce uncertainties on the shape of nitrate gradients observed in the porewater and their response to discharge. However, several field observations at our site (Leote et al. 2008, Rocha et al. 2009) support the assumption of the seepage being predominantly vertical. Seepage at the upper levels of the beach is substantially different in terms of salinity and solute content when compared with the lower levels affected by SGD. Nevertheless, influence of the upper levels in the solute distribution at the lower levels was not identified. With significant horizontal water movement, the higher and unchanged salinity at the upper levels should promote salinity gradients in the lower levels, especially in the upper cm where, at the site, hydraulic conductivity is higher (see Rocha et al. 2009). Instead, salinity profiles in the area affected by SGD were vertically homogeneous when seepage peaked. Moreover, in this more permeable layer close to the sediment–water interface, the lower nitrate content of the upper levels would dilute the nitrate content in the lower levels. Instead, nitrate concentration significantly peaks at the sediment–water interface. Finally, the under saturation of the upper part of the beach when SGD is at maximum avoids significant hydraulic gradient in the upper levels to promote significant horizontal water movement (see Rocha et al. 2009 for a more extensive discussion of this point). Thus, under vertical seepage of salinity-uniform groundwater, vertical solute gradients are clearly linked to benthic reactivity.

Strong depth gradients of dissolved inorganic nitrogen (DIN = NO_3^- + NO_2^- + NH_4^+) and salinity were identified on porewater profiles taken during sediment exposure at low tide. Typical transient DIN profiles (November 2005) are shown in Fig. 2,

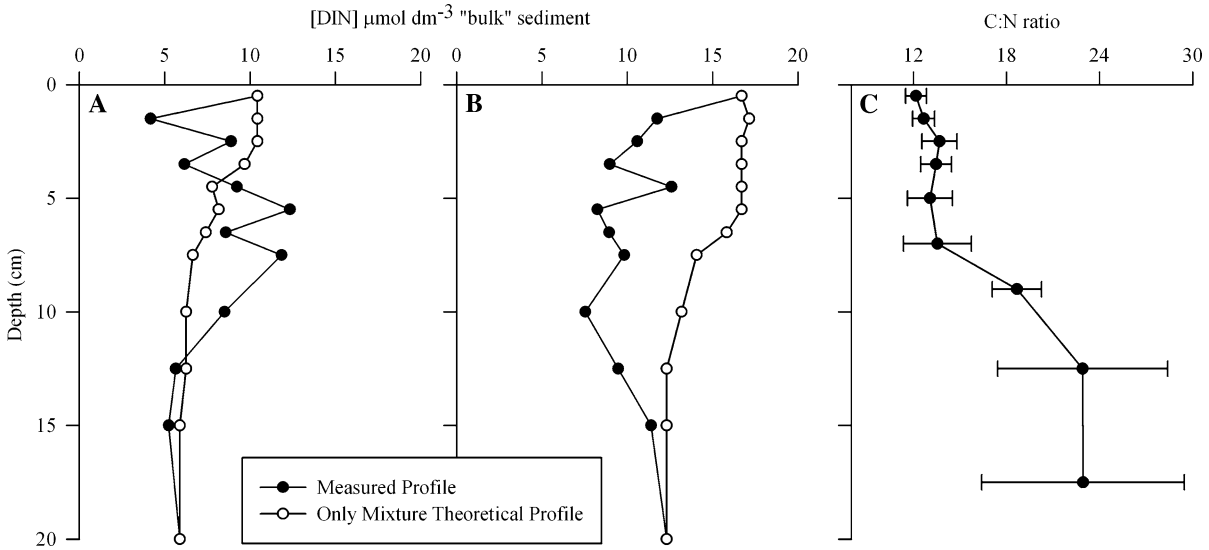

Fig. 2 **a** and **b** Typical dissolved inorganic nitrogen (*DIN*) distribution on porewater affected by submarine groundwater discharge (*SGD*) measured on November 2005 (*black*) along with theoretical only-mixture profiles (*white*). **c** Mean C:N molar ratio of organic matter into the sediment studied on March 2006, corresponding to four profiles taken. Sampled sediment is located at Praia de Faro, South of Portugal. See "Methods" for sampled place description

together with the mean C/N molar ratio of organic matter (March 2006) at the same depth scale. Three different reactive zones may be identified by comparing the measured DIN profiles with the theoretical mixing curve (using salinity as conservative tracer of mixing throughout the vertical distance sampled in situ; Bao-dong and Brockmann 2005; Fig. 2) and with the bulk organic matter C/N ratio depth profile: a) The deeper layer (from 20 to 15–12 cm depth) characterized by showing no significant deviation between mixing-only and measured DIN profiles. On that zone, the C/N ratio depth gradient remained constant, suggesting a relatively invariant refractory organic matter pool; b) An intermediate zone (from 15–12 to 3 cm depth) showing strong segregation between the measured DIN profiles and the theoretical distribution as calculated by the mixing curves. This intermediate layer was also distinguishable by a sharp change in the C/N depth gradient, coincident with permanent depletion of nitrate (see the Results section); Finally, c) The top layer (between 3 cm depth and the sediment–water interface), characterized by DIN and nitrate distributions evidencing peaks against a uniform salinity gradient (see Fig. 2 and Results section). Bulk organic matter C/N ratios persisted here at the lowest values found within the whole profile.

Thus the conceptual reaction zonation to construct the model was based on the discrimination of the sediment reactivity areas into three depth horizons: a nitrification layer (nitrogen oxidation) at the surface, a nitrate reduction layer below that, and a third, non-reactive layer underlying the two (Fig. 3).

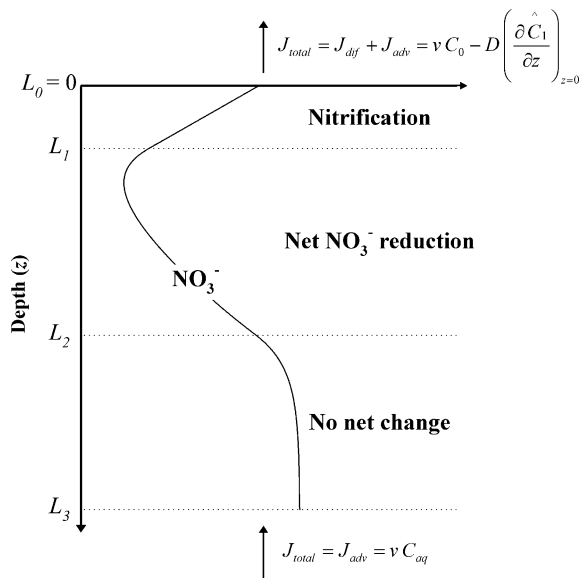

Fig. 3 Schematic view of the three-layer model formulation resulting from the conceptual analysis; distribution of layers, boundary fluxes and theoretical nitrate distribution on the porewater are shown

Model formulation

General formulation and solution

The diagenetic problem was further simplified to a vertical-flow tubular reactor scheme. Transport processes included in the model formulation were molecular diffusion, mechanical dispersion and advective transport. Molecular diffusion and mechanical dispersion were modeled as a single term, dubbed "effective dispersion", and defined as the sum of the dispersive and the diffusive terms, viz: $D_{ef} = D_{if} + D_{\mathrm{isp}}$ (Roychoudhury 2001). The NO_3^- diffusion coefficient in free water solution was calculated using the temperature-dependent parameterization suggested by Boudreau (1997). It was further corrected with the tortuosity in order to calculate the apparent molecular diffusion coefficient in the sediment, thus accounting for the presence of the solid phase ($D_{if} = D_{\mathrm{molec}}/\theta^2$; Berner 1980). Because the modeled medium consisted mostly of sand, Archie's Law was used to calculate the tortuosity from the porosity, thus obtaining $D_{if} = \phi D_{\mathrm{molec}}$ for the apparent diffusion coefficient in the sediment. Mechanical dispersion was included in the model formulation by using the pore-scale solution described by Bijeljic and Blunt (2006), $D_{\mathrm{isp}} = P_e^{1.2}$, where $P_e = vL/D_{\mathrm{molec}}$, P_e being the nondimensional Peclet number resulting from the ratio between the time-scales of advective and diffusive transport, and where v is the advective velocity and L is the characteristic pore length. According to Roychoudhury (2001), mean grain size diameter is a good proxy for characteristic pore lengths in sandy sediments. Since the simulations performed by Bijeljic and Blunt (2006) are designed at the pore scale (60 × 60 pores networks, 3 × 3 cm in our case), they obtained identical results with longer pore networks (up to 4000 pores), thus being appropriate for the 20 cm depth explored here.

For the purpose of this modeling exercise, advective transport of NO_3^- was assumed to be exclusively the result of the vertical seepage flow when the sediment was exposed (Horn 2002; Taniguchi et al. 2006; Rocha et al. 2009). This process is included on the model formulation as v, the velocity of the porewater with respect to the sediment particles, since the presence of the solid phase is accounted for by using the bulk NO_3^- concentration. The reactive processes to be included were divided into nitrification and nitrate reduction. Nitrification was assumed to take place close to the surface, with zero-order kinetics in relation to the NO_3^- concentration. In order to simplify the formulation to a single species model, independence of nitrification rates from ammonium concentration was also assumed, based on the characteristic low K_m for nitrification found on controlled systems (see compilation made by Sheibley et al. 2003). The potential organic matter limitation of benthic bacterial processes could also increase the likelihood of alternative metabolic pathways being present, including dissimilatory nitrate reduction to ammonium (DNRA), anaerobic ammonium oxidation (ANAMMOX) or oxygen-limited autotrophic nitrification–denitrification (OLAND) (Hulth et al. 2005; Bowen et al. 2007; Brandes et al. 2007; Kroeger and Charette 2008). For the purpose of this study, the term "nitrate reduction" describes any process responsible for the depletion of NO_3^- following first-order kinetics with respect to NO_3^- concentration. Finally, and since the distribution of organic matter and nitrate at our site suggests that constraints to nitrate reduction with depth are possible (Fig. 2, results section), we included a third model layer as an optional, non-reactive zone with respect to nitrate.

The porosity varies with depth, thus implying another depth-dependent parameter to be inserted into the model. This dependence (and thus the presence of the solid phase) was included by expressing the constitutive equations in relation to the "bulk" concentration of NO_3^- ($\hat{C}(z) = \varphi(z)C(z)$, Boudreau 1997).

Based on this set of assumptions, the diagenetic equations for the three-layer model were established, based on the general formulation of Advection–Dispersion-Reaction (ADR) models, as follows:

Nitrification layer:

$$\frac{\partial}{\partial z}\left(D_{ef}\frac{\partial \hat{C}_1(z)}{\partial z}\right) - \frac{\partial}{\partial z}\left(v\hat{C}_1(z)\right) + K_n = \frac{\partial \hat{C}_1}{\partial t}$$

NO_3^- reduction layer:

$$\frac{\partial}{\partial z}\left(D_{ef}\frac{\partial \hat{C}_2(z)}{\partial z}\right) - \frac{\partial}{\partial z}\left(v\hat{C}_2(z)\right) - K_d\hat{C}_2(z) = \frac{\partial \hat{C}_2}{\partial t}$$

Non-reactive layer:

$$\frac{\partial}{\partial z}\left(D_{ef}\frac{\partial \hat{C}_3(z)}{\partial z}\right) - \frac{\partial}{\partial z}\left(v\hat{C}_3(z)\right) = \frac{\partial \hat{C}_3}{\partial t}$$

with K_n as the nitrification rate (nmol cm^{-3} h^{-1}), K_d the NO_3^- reduction rate constant (h^{-1}) and z the sediment depth (cm).

The oscillatory nature of the system, along with its observed reproducibility, was used to postulate a pseudo-stationary state in order to solve the system of differential equations. Thus, we assume that during peak discharge from the beach, a stationary state ($\partial C/\partial t = 0$) is reached. Due to the harmonic behavior of the tide, and consequent reproducibility of the seepage event, this behavior is verified every tidal cycle.

Amongst the possible boundary conditions for a finite sediment column, we chose to define the NO_3^- concentrations at the limits of the model domain (i.e., $\hat{C}_1(0) = C_0$ for the sediment–water interface and $\hat{C}_3(L_3) = C_{aq}$ for the concentration at the lower boundary). The continuity conditions imposed to solve the problem analytically were based on the identity of concentrations and fluxes across the interfaces of the domain:

$$\left.\frac{\partial \hat{C}_2(z)}{\partial z}\right|_{z=L_2} = \left.\frac{\partial \hat{C}_3(z)}{\partial z}\right|_{z=L_2} \text{ and } \hat{C}_2(L_2) = \hat{C}_3(L_2) \text{ for } L_2$$

$$\left.\frac{\partial \hat{C}_1(z)}{\partial z}\right|_{z=L_1} = \left.\frac{\partial \hat{C}_2(z)}{\partial z}\right|_{z=L_1} \text{ and } \hat{C}_1(L_1) = \hat{C}_2(L_1) \text{ for } L_1$$

where L_2 represents the depth boundary between the NO_3^- reduction and non-reactive layers (cm) and L_1 is the depth boundary between the nitrification and NO_3^- reduction layers (cm) (see Fig. 3). The analytical solution of the problem for each layer was obtained by solving the differential equations and using the continuity and boundary conditions in order to obtain the integration constants, viz:

Layer 1 (from $z = 0$ to $z = L_1$):

$$\hat{C}_1(z) = \frac{1}{BvH} \left(\begin{array}{l} 2Ae^{\frac{L_1(v+\omega)}{2D_{ef}}}\left(-1 + e^{\frac{zv}{D_{ef}}}\right)v\omega \\ +B\left(K_n\left(-4D_{ef}\left(-1 + e^{\frac{zv}{D_{ef}}}\right) + zH - L_1v\right) - C_0v(v-H) + (K_nL_1 + C_0v)\left(e^{\frac{zv}{D_{ef}}}(v-\omega) + \omega\right)\right) \end{array} \right)$$

Layer 2 (from $z = L_1$ to $z = L_2$):

$$\hat{C}_2(z) = \frac{1}{vBCH}\left(e^{\frac{z(v-\omega)}{2D_{ef}}}\left(\begin{array}{l} 2BC_{aq}e^{\frac{L_2(v+\omega)}{2D_{ef}}}v^2H \\ -A\left(2B + Cv\left(\left(e^{\frac{z\omega}{D_{ef}}} - e^{\frac{L_1(v+\omega)}{D_{ef}}}\right)(v-\omega) - \left(e^{\frac{L_1\omega}{D_{ef}}} - e^{\frac{L_1v+z\omega}{D_{ef}}}\right)(v+\omega)\right)\right) \end{array} \right)\right)$$

Layer 3 (from $z = L_2$ to $z = L_3$):

$$\hat{C}_3(z) = \frac{1}{v^2BCH}\left(\begin{array}{l} BC_{aq}v^2H\left(C - \left(e^{\frac{L_3\omega}{D_{ef}}} - e^{\frac{zv}{D_{ef}}}\right)(v-\omega)\right) + Ae^{-\frac{L_2(v+\omega)}{2D_{ef}}}\left(e^{\frac{L_3\omega}{D_{ef}}} - e^{\frac{zv}{D_{ef}}}\right) \\ \left(\begin{array}{l} B(v-\omega) + Cv\left(\begin{array}{c} 2D_{ef}K_d\left(-1 + e^{\frac{L_1v}{D_{ef}}}\right)\left(e^{\frac{L_1\omega}{D_{ef}}} - e^{\frac{L_2\omega}{D_{ef}}}\right) \\ +v\left(e^{\frac{L_1(v+\omega)}{D_{ef}}}(v-\omega) - e^{\frac{L_2\omega}{D_{ef}}}(H - v + \omega)\right) \end{array} \right) \end{array} \right) \end{array} \right)$$

With support constants defined as follows:

$$\omega = \sqrt{4D_{ef}K_d + v^2};$$

$$H = v - \omega + e^{\frac{L_1v}{D_{ef}}}(v+\omega);$$

$$C = e^{\frac{L_3v}{D_{ef}}}(v-\omega) + e^{\frac{L_2v}{D_{ef}}}(v+\omega);$$

$$A = Ce^{-\frac{L_1(v-\omega)}{2D_{ef}}}\left(e^{\frac{L_1v}{D_{ef}}}\left(D_{ef}K_n - v(K_nL_1 + C_0v)\right) - D_{ef}K_n\right) + C_{aq}e^{\frac{L_2(v+\omega)}{2D_{ef}}}v^2H$$

and

$$B = 2vD_{ef}K_d\left(-1 + e^{\frac{L_1v}{D_{ef}}}\right)\left(e^{\frac{L_2v}{D_{ef}}} - e^{\frac{L_3v}{D_{ef}}}\right)\left(e^{\frac{L_1\omega}{D_{ef}}} - e^{\frac{L_2\omega}{D_{ef}}}\right) + v^2\left(\left(e^{\frac{L_2(v+\omega)}{D_{ef}}} - e^{\frac{(L_1+L_3)v+L_1\omega}{D_{ef}}}\right)(v-\omega) + \left(e^{\frac{(L_1+L_3)v+L_2\omega}{D_{ef}}} - e^{\frac{L_2v+L_1\omega}{D_{ef}}}\right)(v+\omega)\right)$$

Free-boundary solution

To improve the predictive capabilities of the model, an additional boundary condition was used to derive

an expression allowing for the prediction of the surface boundary concentration (C_0) by the model. This was obtained by simplification of the expression deriving the mass balance for the top layer (i.e., from $z = 0$ to L_1). Assuming that the difference between the dispersive fluxes at both limits of the layer $D_{ef}\left(\partial\hat{C}_1(z)/\partial z\right)_0 - D_{ef}\left(\partial\hat{C}_1(z)/\partial z\right)_{L_1}$, are negligible by comparison with the advective and reactive terms when seepage is dominant (advective dominated system), the following expression for the concentration of NO_3^- at the sediment–water interface may be obtained:

$$C_0 \cong (1/v)\left(v\hat{C}_1(L_1) - K_n L_1\right).$$

Substituting $\hat{C}_1(L_1)$ and solving for C_0, we obtain a free-boundary solution for the problem, viz:

$$C_0 = \frac{BK_n\left(L_1(v-\omega) - 4D_{ef}\right) + 2v\omega\left(CK_n e^{\frac{L_1\omega}{D_{ef}}}\left(e^{\frac{L_1 v}{D_{ef}}}\left(L_1 v + D_{ef}\right) - D_{ef}\right) + v^2 HC_{aq} e^{\frac{(L_1+L_2)(v+\omega)}{D_{ef}}}\right)}{v\left(2v^2\omega C e^{\frac{L_1(v+\omega)}{D_{ef}}} - B(v-\omega)\right)}$$

This approximation is only valid when advection is the dominant transport process for the domain (e.g., during sediment exposure and when groundwater seepage is at its peak).

Results

Range of applicability of the free-boundary solution

In order to test the validity of the simplification for the free-boundary solution, the ratio between the extended mass balance for the surficial reactive layer and the simplified one (Ψ) was used:

$$\Psi = \frac{v\hat{C}_1(L_1) - K_n L_1}{v\hat{C}_1(L_1) - K_n L_1 + D_{ef}\left(\left(\partial\hat{C}_1(z)/\partial z\right)_0 - \left(\partial\hat{C}_1(z)/\partial z\right)_{L_1}\right)}$$

The range of parameters for which this ratio became close to unity, with a finite up-flow velocity, was explored. As an additional quality estimator for the results of the free-boundary solution, mass conservation was checked by systematically calculating the model-based mass balance for the whole domain.

Two important nondimensional parameters, the Peclet number, P_e, and the Damköhler number, D_a, were used both for the test of the free-boundary solution and for subsequent exploration of model results, at each of the modeled reaction domains. Damköhler numbers result from the ratio between the temporal scales of reaction and transport (e.g., Carleton 2002). We used the following expressions:

$$D_{a1} = \frac{K_n L_1^3}{D_{ef}\int_{L_1}^{0}\hat{C}_1(z)\partial z}$$

for the Damköhler number representative of the nitrification layer, and

$$D_{a2} = \frac{K_d(L_2 - L_1)^2}{D_{ef}}$$

for the Damköhler number representative of the NO_3^- reduction layer.

The test results of the simplification applied to obtain the free-boundary solution showed high stability. No significant deviation (within 5%) of the function used as convergence criterion (Ψ) was found for the main tested parameters (data not shown). In fact, Ψ maintained values close to 1 whilst P_e, D_{a1} and D_{a2} were modified, implying the pertinence and physical coherence of our simplification. Some deviation was observed only for P_e values on the extreme low-end of the applied range (P_e around 1), in agreement with the premises of the modeled system, which stated that this was an advection dominated system. This deviation becomes more obvious when manipulating the width of the nitrate reduction layer (distance between L_2 and L_1, Fig. 4).

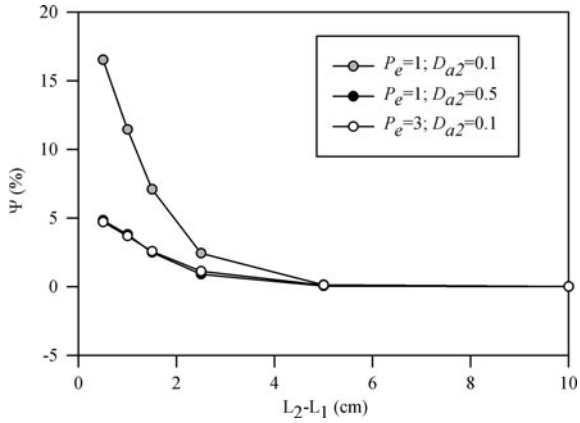

Fig. 4 Results of the test performed (Ψ) over the free-boundary solution approximation: Stability of simplification within the nitrate reduction layer length is shown. Influence of advective regime (hydrological Peclet number) and nitrate reduction rates (in the form of dimensionless Damköhler numbers) are crucial at the lower end of the applicated range

Ψ became unstable for widths down to 2 cm when P_e number was in the extreme low-end of the transition zone between a diffusion dominated and a pure advective regime (Bijeljic and Blunt 2006). Exploring the instability at $P_e = 1$, larger deviations were found for decreasing nitrate reduction rates (in the form of D_a numbers, Fig. 4). These deviations disappeared at higher P_e numbers and/or higher nitrate reduction rates.

Sensitivity analysis

A sensitivity analysis was performed to determine the influence of each different model input parameter both on the NO_3^- concentration gradients and on the derived surface fluxes. The results were used not only to identify the most important parameters to be determined during future on-site fieldwork, but also to obtain further information on the key variables controlling the NO_3^- distribution in the porewater and the magnitude of the NO_3^- seepage fluxes under the described conditions. Input parameters were varied across their realistic ranges, based on typical literature values and own data obtained in situ, but excluding values outside the range of applicability of the model (see previous section).

The nondimensional ratio between NO_3^- concentrations at both limits of the modeled domain, (i.e., C_0/C_{aq}), was used in order to determine the influence of each model parameter on the NO_3^- profile. The function $S(x, y) = (\partial x/x)/(\partial y/y)$ was used as an estimator of the sensitivity of the resulting upper-boundary fluxes (x) to changes imposed on each parameter (y) (Jørgensen 1994; Schauser et al. 2006). The function $S(x, y)$ was used in its discrete form. At each parameter value, 5% of change was induced to subsequently follow how upper-boundary fluxes reacted to those changes. This process was performed covering the whole parameter range inside the applicability of the model. The use of non-dimensional D_a numbers allows the evaluation of the effect of changing reaction rates normalized to their most important physical constraints in-loco, i.e., spatial coverage of a given mechanism or relative weight of diffusion with regards to advection. Therefore, in order to minimize temporal and spatial interdependences of the model parameters in the sensitivity evaluation, the sensitivity analysis was performed using nondimensional D_a and P_e parameters.

The most important parameters controlling the NO_3^- distribution within the model domain were the reaction rates and the advective regime (Fig. 5a). Low reaction rates at low seepage velocities (D_a numbers lower than 0.2) can significantly change the NO_3^- concentrations inside the model domain (Fig. 5a). For example, setting D_{a1} to a value close to 0.5 at low P_e values ($P_e = 3$) can increment the nitrate concentration in the profile up to 100% from the initial amount of nitrate entering at the lower depth limit (C_{aq}). Advective velocity showed an important effect over those changes, by enhancing NO_3^- addition to the top layer by nitrification and increasing NO_3^- depletion by nitrate reduction (in terms of constant nondimensional D_a, Fig. 5a).

Analysis of the influence of the different model parameters in the resulting upper-boundary fluxes ($S(x, y)$, Fig. 5b) confirmed the crucial role of reaction rates and advective velocity; fluxes were always highly sensitive to changes in P_e ($S(x, y) \geq 1$), meaning that the upper boundary fluxes at least co-varied with changes in P_e. P_e and surface fluxes kept co-varying when reaction rates were low ($S(x, y) = 1$). This situation changes when higher D_a numbers are imposed, whereby changes to the P_e number induce larger changes on upper boundary fluxes ($S(x, y) > 1$, Fig. 5). Sensitivity analysis was also performed over the input nitrate concentration

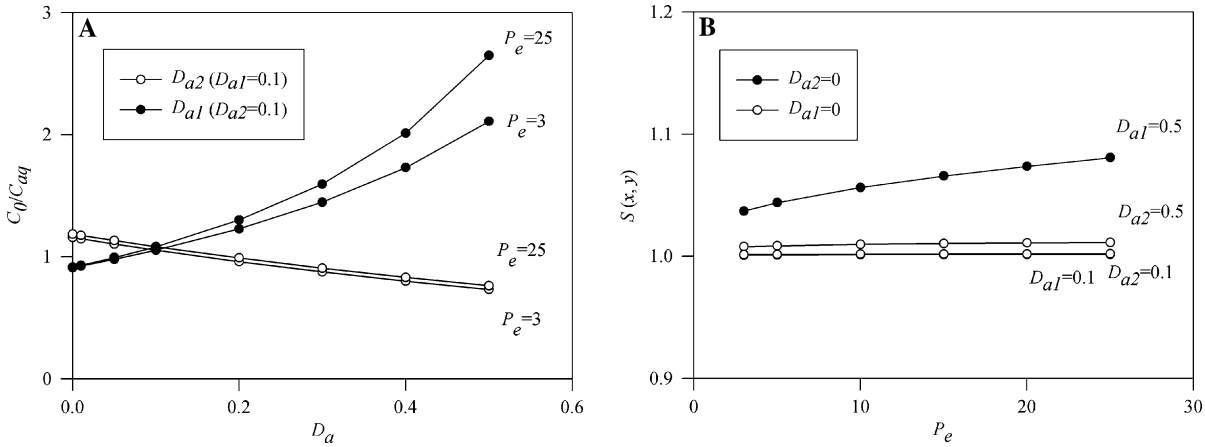

Fig. 5 **a** Influence of reaction rates (in the form of dimensionless Damköhler numbers) and advective regime (hydrological Peclet number) on net NO_3^- transformation capacity inside the model domain (C_o/C_{aq}). **b** Sensitivity [S (x,y)] of the predicted interface fluxes calculated using the model at changing reaction rates (in the form of Damköhler numbers) and changing advective regime (in the form of Peclet number). Both Damköhler and Peclet numbers were used inside the model application range

(C_{aq}) and effective dispersion. Sensitivity was always low for those parameters (lower than 0.5, data not shown).

Model description of field data

Model input parameters

Advective velocity was calculated from in situ seepage meter data. The measured seepage rates were integrated throughout a 1 h time interval centered at the time at which the profile was sampled. As a result of the field work strategy, more than one seepage meter located beside each profiler produced data for subsequent use in the integrations. Temperature for the calculation of diffusion coefficients was also obtained by integrating temperature data obtained from the seepage meters during the same period. NO_3^- concentration of the water entering the model domain (C_{aq}) was fixed using the in situ concentration measured at the lower end of each profile. The model was used to fit the in situ NO_3^- concentration profiles and extract the reaction rates, layer lengths and fluxes. To ensure that NO_3^- gradients were mainly caused by reaction and the constant seepage of water, only profiles with a salinity depth-variance lower than 1 ppt, the error associated with hand-refractometer determinations of salinity, were used in this analysis. The average grain size was used to calculate P_e in accordance with Roychoudhury (2001). Model-derived porewater NO_3^- concentration profiles were fitted to the data, by minimizing the sum of squared differences between each other, with the aid of the Solver routine (Microsoft Excel). To check the quality of the adjustment, the linear correlation between the two data sets was used (Berg et al. 1998). Finally, in order to compare the quality of fit for different profiles, the standard deviation (s) of the fits was normalized to the integrated concentration of the whole domain, by using

$$U(\%) = \frac{\left(\int_{L_3}^{0} \hat{C}(z)\partial z/L_3\right) - \sqrt{s^2}}{\int_{L_3}^{0} \hat{C}(z)\partial z/L_3} \times 100$$

All profiles used in this study were obtained in conditions fitting the range of applicability of the model. The selected profiles were chosen amongst all available profiles in order to show high temporal distribution and model response to different input parameters: profiles are differentiated by advective velocity (hence dispersion coefficient associated to the advective motion), porewater salinity and thus NO_3^- concentration entering in the domain (C_{aq} and associated flux), as well as apparent vertical

NO_3^- gradients. They also differed on the output results in terms of apparent reaction rates, reactive layer length and number of layers employed in the fitting procedure (dependant on the inclusion or lack thereof of the optional non-reactive layer in depth).

Fit Results

The measured profiles, relevant salinity profiles, and associated model fits are shown in Fig. 6. Table 1 shows the values of the parameters used to quantify the goodness of model fits and the depth integrated standard deviation of the measured salinity profiles. The standard deviation of salinity in the profiles was always lower than 1 ppt (<0.7 ppt), thus meeting the criterion used to ensure a homogenized column in terms of mixing. The modeled NO_3^- profiles fitted the measured data with high correlation; both the linear correlation and the U (%) convergence criterion were always higher than 70%, and usually above 90%.

Sediment–water fluxes extracted from the model fits to the data (Table 2) were plotted with respect to those obtained from the seepage meters (Fig. 7). No

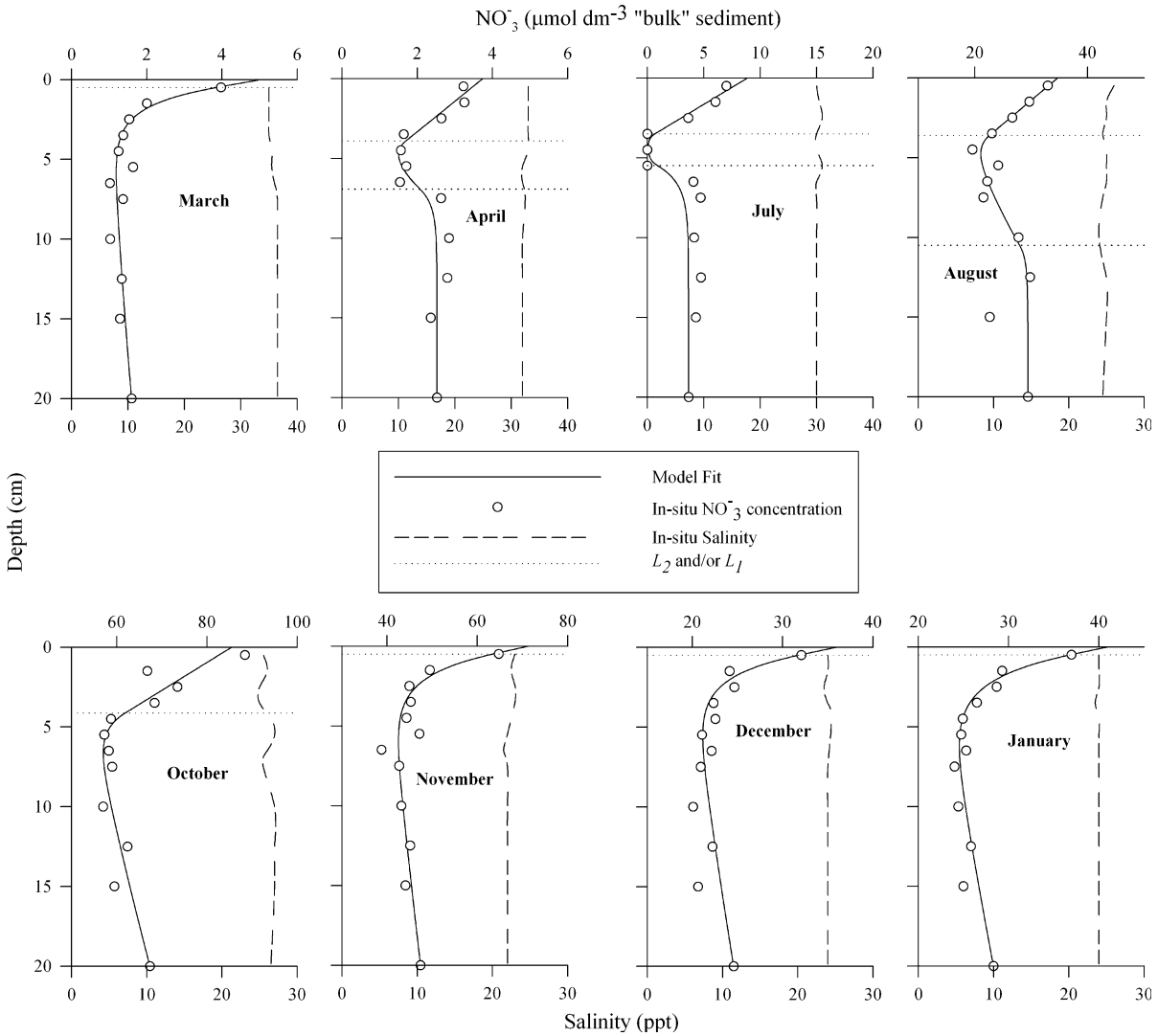

Fig. 6 Measured NO_3^- profiles plotted together with modeling results. The concomitant measured salinity profiles are also shown

Table 1 Model fit results: standard deviation and linear correlation (%) of the model fit to the measured NO_3^- distribution in the porewater, standard deviation of the fits normalized to the integrated concentration of the profile, *U* (%), and standard deviation of measured salinity porewater profiles used to ensure the homogeneous seepage of the mixed water

	SD	Linear correlation (%)	*U* (%)	Salinity SD (ppt)
March	0.19	96.84	87.21	0.60
April	0.25	91.19	89.02	0.42
July	0.89	93.32	72.40	0.30
August	2.25	84.19	91.37	0.43
October	3.81	90.08	93.76	0.67
November	2.10	93.87	95.23	0.38
December	1.24	91.66	94.39	0.16
January	0.85	96.97	96.68	0.10

direct 1:1 relationship between each other was found, mainly because integrated salinity profile values from seepage meters and profiles differed significantly (see Table 2). This might be explained by the dead volume inside the seepage meters leading to a delay between brackish water arrival at the chamber and sampling time, and the fact that the spatial heterogeneity effect on the seepage meter fluxes was minimized by using two or three chambers per position. However, significant linear correlation between NO_3^- concentration and salinity was evident on all our seepage meter data (Leote et al. 2008). This correlation was used to adjust the NO_3^- concentration at the seepage meters for that expected from each porewater salinity profile, allowing uniformization of the predicted and measured fluxes (Fig. 7). With this correction, a good linear regression ($R^2 = 0.8672$) was obtained, with a slope close to unity (0.9948), thus convincingly linking the predicted boundary fluxes to the ones measured in situ.

The model-derived profiles accounted for the principal NO_3^- distribution patterns observed on the in situ vertical profiles (Fig. 6). Transport input parameters used (P_e numbers and D_{ef}) along with reaction rates and reaction layer depths derived from model fits to the data are shown on Table 3. P_e numbers were in the range of the power law description of dispersion (Bijeljic and Blunt 2006), and together with the NO_3^- reduction layer length ($L_2 - L_1$), high enough to permit the use of the free-boundary approximation. Apparent nitrification rates, derived from the model, ranged from 0.05 to 1.9 mmol m^{-2} h^{-1} and apparent NO_3^- reduction rates from 0.03 to 2.14 mmol m^{-2} h^{-1}.

Indication of the existence of limits to nitrate reduction at depth was also found on April, July and August (requiring the inclusion of the third layer, Table 3). In these cases, the simplified 2-layer model fit ($L_2 = L_3$; Fig. 8), always showed higher standard deviation to the measured NO_3^- profile than the 3-layer model fit. A one-tailed F test was used to test

Table 2 Comparison between measured and modeled fluxes: integrated salinity over the measured profiles, salinity measured in the seeping water with the seepage meters, modeled fluxes of NO_3^- at the lower limit (L_2) and at the sediment–water interface, and fluxes of NO_3^- measured with seepage meters are shown

	Profile salinity (ppt)	Seepage meters salinity (ppt)	Flux at L_2 (mmol m^{-2} h^{-1})	Modelled sed-water flux (mmol m^{-2} h^{-1})	Measured sed-water flux (mmol m^{-2} h^{-1})	Measured flux corrected by salinity (mmol m^{-2} h^{-1})
March	36.12	29.49	−0.09	−0.11	−0.35	−0.10
April	32.26	33.68	−0.06	−0.08	−0.04	−0.09
July	30.11	31.90	−0.36	−0.60	−0.28	−0.47
August	24.76	26.44	−1.18	−1.27	−1.18	−1.55
October	26.42	23.62	−5.53	−6.35	−4.17	−3.37
November	22.16	30.38	−7.78	−7.80	−3.39	−7.08
December	24.00	33.23	−2.10	−2.00	−0.98	−2.25
January	23.98	23.24	−9.94	−9.22	−9.35	−11.68

As result of the differences in salinity between the measured profiles and the seepage meters data, a salinity correction of the seepage meters data was performed allowing direct comparison with the modeled fluxes

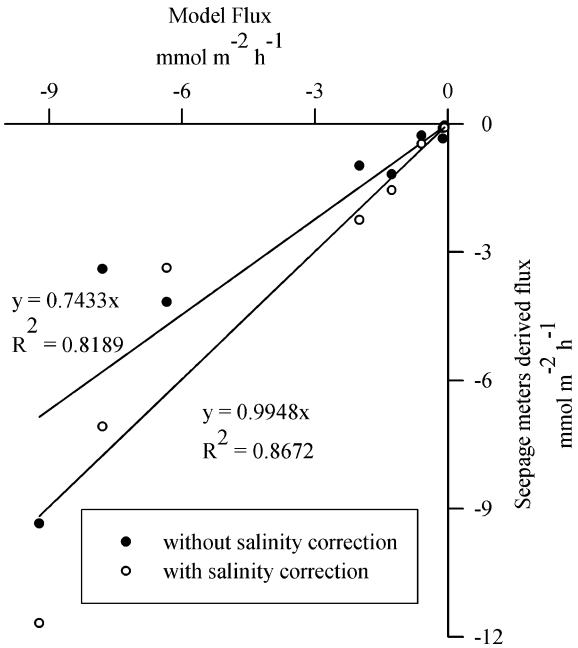

Fig. 7 Model-predicted interfacial seepage fluxes plotted against measured fluxes on site with seepage meters (*black dots*). Salinity correction of field fluxes to be comparable with the exact depth-averaged salinity for the porewater profiles used in the modeling procedure are also shown (*white dots*)

the statistical significance of the inclusion of the third layer on the model fits to the real data (Soetaert et al. 1996; Berg et al. 1998). The null hypothesis tested in this case was that the inclusion of the third, non-reactive layer did not significantly improve the model fit to the field-measured data, in comparison with the simpler two-layer model ($L_2 = L_3$). When applying the F-test between the 3-layer model and the equivalent 2-layer model, statistical significance of the inclusion of the third layer was found on profiles from April to July, on a 99% confidence interval, while the more complex three-layer model application did not significantly improve the fit on August.

Discussion

The validity and applicability of the model with the free boundary solution approximation was tested via multiple methods. The mass balance performed within the entire domain of the model was always checked and always showed coherence. The results of testing the simplification (Ψ) showed the high stability of the primary assumption, e.g., an advection dominated system. Moreover, the free-boundary solution showed also high stability for different spatial scales, reactive rates, layer lengths and input parameters. Some instability of the free-boundary approximation at low P_e numbers (inside the lowest transition zone between diffusive to advective dominated regime, i.e., $1 < P_e < 3$) was found. At this transition zone, the function Ψ deviated significantly for NO_3^- reduction layer lengths ($L_2 - L_1$) smaller than 2 cm. This deviation disappears at higher P_e numbers or when high reaction rates are imposed, which suggests the need of a good-sized reactor for stability of the system.

Table 3 Advective velocity obtained from the seepage meters (in the form of the nondimensional P_e number) used in the modeling process as input parameter is shown

	P_e	D_{ef} (10^{-4} m^2 h^{-1})	D_{a1}	Nitrification rate (mmol m^{-2} h^{-1})	L_1 (cm)	D_{a2}	Nitrate reduction rate (mmol m^{-2} h^{-1})	L_2 (cm)
March	4.76	6.52	0.26	0.06	0.50	0.45	0.04	20
April	2.15	2.52	0.76	0.05	3.91	0.82	0.03	6.93
July	7.50	11.24	1.71	0.79	3.49	20.58	0.55	5.49
August	2.93	3.66	0.42	0.49	2.86	0.42	0.39	10.50
October	6.64	9.71	0.32	1.90	4.13	0.22	1.09	20
November	13.99	23.72	0.12	1.27	0.50	0.17	1.25	20
December	8.03	12.19	0.12	0.34	0.49	0.23	0.44	20
January	29.78	58.73	0.11	1.42	0.50	0.23	2.14	20

Effective dispersion coefficient calculated from diffusion coefficient and P_e number at each profile modeled is also shown, along with parameters obtained from the fit procedure: reaction rates in the form of reaction rates the nondimensional D_a numbers together with depth distribution of reaction layers

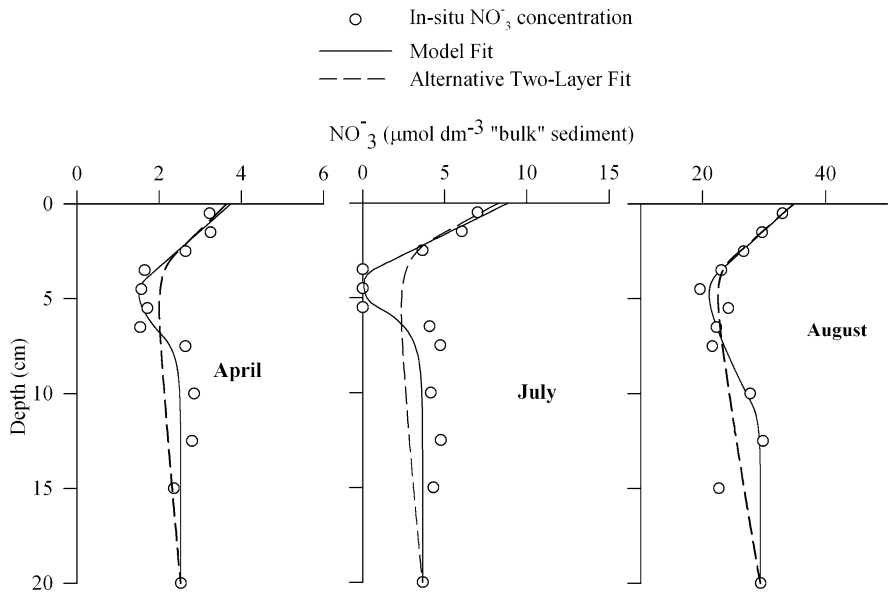

Fig. 8 Model fits with and without inclusion of a non-reactive layer, when NO_3^- profiles evidence no gradient in concentration near the lowermost end of the domain; testing the statistical significance of inclusion of non-reactive layer on modeled field data

The performed sensitivity analysis showed that the main parameters controlling both the NO_3^- porewater distribution and seepage fluxes are the advective velocity and the reaction rates. Advective velocity is the forced parameter and thus the dominant factor of both the NO_3^- distribution in porewater and the cross-interface fluxes. The boundary fluxes depend strongly on the seepage rate and this dependence is well defined on this analysis. However, since the importance of the reaction rates in affecting the magnitude of the interfacial fluxes is shown, the NO_3^- concentration arriving at the domain (C_{aq}) could be a dominant parameter controlling the surface discharge of NO_3^- only when low benthic reactivity is present, but looses importance when higher potential reaction rates are possible. Thus, C_{aq} is an important parameter to characterize the system, but does not necessarily determine the solute flux to the external environment. Overall, analysis of the sensitivity of model output to different benthic reactivities, as well as discharge rates, suggest that the sandy environment can significantly change the final concentration and load of NO_3^- into the lagoon. Therefore, in order to predict the impact of SGD in the receiving environment, a good knowledge of benthic biogeochemistry at the seepage face is necessary, particularly near the sediment–water interface.

The description of measured benthic NO_3^- distributions shows the stability of the model and the pertinence of the assumptions underpinning its formulation. A variety of modeled profiles, characterized by different P_e numbers, salinities, C_{aq} concentrations and vertical NO_3^- gradients are shown. The model accounted for both overall shape and curvature, reproducing the measured depth profiles with high correlation. Even including the possible sampling artifacts like interference between sampled horizons, and the dynamism of the benthic environment, the high values of the fit correlations evidenced the quality of the adjustment. In addition, the comparison between the measured and model-derived fluxes adds to the reliability and predictive capability of the model. This comparison offered a close to 1 relationship with a high linear regression coefficient even taking into account the potential artifacts associated with the operation of seepage meters, extensively discussed in the methodology section.

During the model development process we approximate the system to a pseudo-stationary state when sediment is exposed within an advective dominated environment caused by vertical submarine groundwater discharge. In order to test the pertinence of our assumption, the advective velocity and NO_3^- fluxes obtained with the seepage meters for the whole exposure period were integrated and checked against the profiles used. The resulting average advective velocity was used as input parameter for the model fit, and the resulting fluxes were plotted against those obtained from the seepage meters (Fig. 9). A

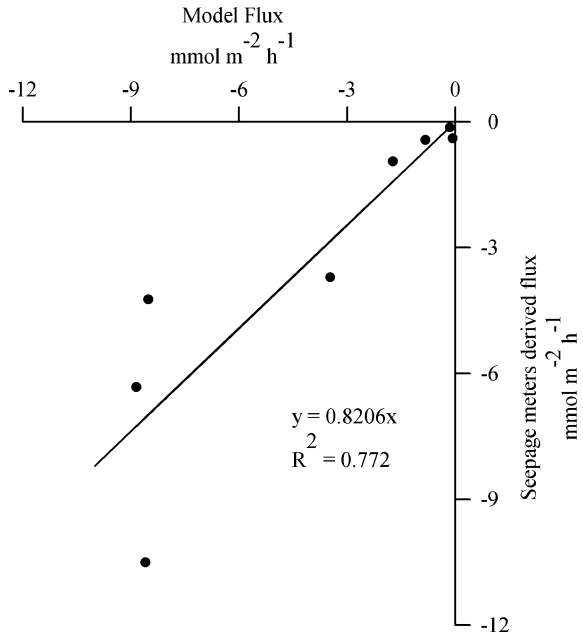

Fig. 9 Pseudo-stationary state assumption tested; model-predicted interfacial seepage fluxes plotted against fluxes measured on site with seepage meters during the whole sediment exposure period

deviation of almost 18% between modeled and measured data was observed. The considerations made on the comparison between modeled and measured fluxes during the main modeling effort are also applicable here. The deviation caused by the November data set, were the overall profile salinity was 22 ppt but the measured salinity on the seepage meters never dropped below 28 ppt during the entire sampled tidal cycle, was particularly noteworthy. Despite that fact, which shows an extreme case of the impact of spatial variability on seepage rates, good agreement between both data sets allowed confirmation of the physical verisimilitude of our pseudo-stationary state assumption during sediment exposure.

Apparent reaction rates (nitrification and nitrate reduction) extracted from the model fits were in the order of 10^{-2}–10^{0} mmol m^{-2} h^{-1}. These are compared to literature values in Table 4. Nitrification rates at our site are comparable with the potential rates found in muddy sediments by Laima et al. (2002) and Dollhopf et al. (2005). For sandy sediments, the mass balances published by Rocha and Cabral in 1998 (at similar latitude) and Usui et al. (2001) where also comparable. Model derived nitrate reduction rates where similar to denitrification rates found in marine muddy sediments (Dollhopf et al. 2005), subtidal sandy sediments (Gran and Pitkänen 1999; Usui et al. 2001) and intertidal sandy sediments at similar latitudes (Rocha and Cabral 1998). However, they are significantly higher than rates measured by Nowicki and Portnoy (1999) and Ueda et al. (2003) on intertidal sandy sediments affected by nitrate-rich groundwater-borne discharge. This discrepancy can be explained by two facts: Firstly, rates determined by Ueda et al. (2003) were obtained from static core incubations (minimal potential denitrification). Because denitrification is usually identified as dependant on the amounts of NO_3^- provided to the reaction zone (first-order kinetics), its rate will depend on the NO_3^- loading of the reactive layer, thus being strongly conditioned by the advective flux. On the other hand, "nitrate reduction" is defined here as any process responsible for the depletion of porewater NO_3^- content in the direction of flow. For example, the work of Kim et al. (1997) showed that heterotrophic denitrification accounted for less than 10% of the total nitrate reduction rate. The environment studied here constitutes an interface link between nitrate-rich low organic content groundwater, benthic reactivity at the seepage zone, and oscillatory sea water infiltration into the subterranean estuary (Moore 1999). The dynamic biogeochemical zonation thus established could limit heterotrophic denitrification and enhance the potential for alternative metabolic pathways, including DNRA, ANAMMOX or OLAND (Bowen et al. 2007; Brandes et al. 2007). Apparent nitrate reduction rates derived from our model accounted for the observed net decay in NO_3^- concentration, but did not discriminate between potential pathways.

In natural porous media with advection dominating interfacial transport and hence solute distribution, the associated dispersivity, being orders of magnitude higher than diffusivity, can also affect the porewater distribution of the solutes (Roychoudhury 2001). Even including the advective motion in calculations based on the porewater nitrate gradients, direct (based on profile concentrations) mass balance approaches neglect the effect of dispersion. Thus, direct mass balances cannot separate the transport effect on NO_3^- gradient shape and reach from the gradients caused by biogeochemical reactivity. When compared with model

Table 4 Typical benthic nitrification and denitrification rates on literature

Place	Sediment type	Nitrification rate (mmol m^{-2} h^{-1})	Method	Denitrification rate (mmol m^{-2} h^{-1})	Method	Reference
Skidaway Island (USA)	Salt marsh	−0.023–0.913[a]	NH_4^+ incubations	0.195–3.228[a]	Acetylene block technique	Dollhopf et al. 2005
Boston Harbor (USA)	Variable (Subtidal)			0.01–0.412	Direct N_2 flux	Nowicki et al. 1997
Marennes-Oléron Bay (France)	Intertidal mudflat	0.79–2.5[a]	Acetylene block technique			Laima et al. 2002
Hiroshima Bay (Japan)	Subtidal, variable	0–0.021[a]	Acetylene block technique	0–0.005[a] (0–0.056)[b]	Acetylene block technique	Kim et al. 1997
Kertinge Nor estuary (Denmark)	Sandy sediment (0.5 m depth)			0.002–0.12[a]	Isotpe paring	Rysgaard et al. 1995
Finland estuary	Variable (Subtidal)			0.007–1.26[a]	Isotpe paring	Gran and Pitkänen 1999
Tama Estuary (Japan)	Subtidal fine sand and mud	0.246–0.716	Mass balance	0.214–1.26[a]	Isotpe paring	Usui et al. 2001
Sylt Island (Gernany)	Sandy and coarse sandy intertidal sediment	0.001–0.026[a]	Isotpe paring	0–0.011[a]	Isotpe paring	Jensen et al. 1996
Sado estuary (Portugal)	Intertidal exposed sandy sediment	1.2	Mass balance	1.1	Mass balance	Rocha and Cabral 1998
Nauset Mars Estuary (USA)	Intertidal sand/silt flat[c]			0–0.096	Direct N_2 flux	Nowicki and Portnoy 1999
Tokio Bay (Japan)	Sandy beach[c]			0.00045–0.018[a,d]	Acetylene block technique	Ueda et al. 2003
Ria Formosa (Portugal)	Sandy sediment affected by SGD	0.05–1.9[c]	Model fit to real data	0.03–2.14[b]	Model fit to real data	This study

[a] Potential nitrification/denitrification rate

[b] Nitrate reduction rate

[c] Affected by nitrate rich groundwater

[d] Minimal potential denitrification

outputs (Table 5), mass balance calculations lead to an underestimation of NO_3^- reduction potential and an overestimation of nitrification. More so, the direct mass balance approach might originate contradictory interpretation of the overall benthic mediating role over NO_3^- fluxes when compared with the model outputs (notice the contradictory overall sediment interference on NO_3^- fluxes calculated by mass balance and by modeling for December and January). The model successfully explained positive (production) solute gradients close to the sediment surface up to 6 cm depth with nitrification layer lengths of less than 1 cm width (Table 3). In this sense, modeling results show an interesting linkage between both reactive layers; even with significant advective up-flow transport, NO_3^- production in the nitrification layer can feed NO_3^- into the reduction layer below. Hence, the model not only incorporates the effects of advection and dispersion, but may also offer valuable information on the vertical biogeochemical zonation present at the time of profile collection.

Table 5 Apparent reaction rates derived from simple mass balance approach over the NO_3^- profiles used in this study

	Mass balance approach				Current model
	NO_3^- reduction (mmol m^{-2} h^{-1})	Nitrification (mmol m^{-2} h^{-1})	Overall transformation (mmol m^{-2} h^{-1})	L_1 (cm)	Overall transformation (mmol m^{-2} $h^{-1)}$
March	−0.03	0.16	0.127	6.50	0.027
April	−0.02	0.04	0.017	6.50	0.017
July	−0.36	0.68	0.324	3.50	0.241
August	−0.39	0.54	0.142	4.50	0.091
October	−0.82	2.52	1.699	5.50	0.817
November	−1.40	4.20	2.804	6.50	0.020
December	−0.38	1.01	0.629	10.00	−0.096
January	−1.48	4.46	2.976	7.50	−0.717

Overall net transformation obtained by both simple mass balance and modelling approaches is also shown for comparison. Mass balances were performed by using the minimum NO_3^- concentration at each profile as the limit between both reactive layers (L_1 in the conceptual model performed)

The possible existence of different reactive pathways involving NO_3^- processing at benthic locations affected by SGD (Kroeger and Charette 2008), underpin uncertainties regarding the final role of the permeable sediments as modulators of land-derived nutrient inputs to the coastal zone (Rocha 2008; Rocha et al. 2009). In this sense, direct N_2 flux measurements and the use of stable isotopes analysis on both natural samples and controlled systems would supply important information on the relative importance of each pathway, along with the interactions with other elements, biogeochemical kinetics and environmental factors controlling the system (Hamersley and Howes 2005; Pallud et al. 2007; Kroeger and Charette 2008). Identification of the main reactive zone along with the expected overall reactivity could help to improve the design of further laboratory studies, ensuring the dominance of a specific microbial population (Hamersley and Howes 2005; Pallud et al. 2007; Rocha 2008).

With the free-boundary solution presented here, the model is specifically designed for the sediment exposure period, an advective-dominated system. Moreover, it could be used without the proposed free-boundary solution for the sediment–water interface to fit NO_3^- profiles for the steady state diffusion-dominated transport case, when the sediment is flooded and no up-flow of porewater is affecting the system. The concentration at the interface (C_0) in this case is controlled by the overlying water (Vanderborght and Billen 1975). Thus, the solution presented here would be applicable to a variety of cases, crossing the transition from diffusion-dominated to advection-dominated environments, and beyond, to the pure advective transport case scenarios.

Conclusions

We satisfactorily reproduce the porewater NO_3^- distribution in advective-dominated seepage zones by including mechanical dispersion within an ADR model with a free boundary solution. The stability of the model was demonstrated and constrained within the limits set by the applicability of the free-boundary solution. Based on the results of the sensitivity analysis, we show that NO_3^- porewater distribution and surface fluxes could be controlled primarily by the seepage velocity and benthic reactivity. Furthermore, the concentration of NO_3^- arriving at the surface reaction zone might not define the resulting seepage fluxes when important biogeochemical reaction rates are present. Results obtained from the model fits to in situ porewater profiles were analyzed and the reliability of the model outputs was demonstrated. The proposed model may increase the accuracy of reaction rate estimates and geochemical zonation at SGD sites, and be an important aid in preparing further experimental studies of local reaction kinetics affecting nitrate distribution in sediments impacted by groundwater discharge.

Acknowledgments The authors gratefully acknowledge M. Simão, S. Pólvora and C. Moita for their help during fieldwork. The "Laboratório de Análises Químicas" kindly offered the room and spectrophotometer time required for nutrient analysis. Financial support was provided by the

Portuguese Foundation for Science and Technology (FCT) through grant contracts SFRH/BD/39170/2007 (Fellowship to JSPI) and SFRH/BD/38856/2007 (Fellowship to CL), and project O-DOIS: Oxygen dynamics coupled to carbon mineralization in sandy intertidal sediments, contract ref: POCTI/CTA/47048/2002. The two anonymous reviewers and the editor are acknowledged for their constructive comments which helped to improve the earlier draft of the manuscript.

References

Andrade C, Freitas MC, Moreno J, Craveiro SC (2004) Stratigraphical evidence of Late Holocene barrier breaching and extreme storms in lagoonal sediments of Ria Formosa, Algarve, Portugal. Mar Geol 210(1–4):339–362. doi:10.1016/j.margeo.2004.05.016

Bao-dong W, Brockmann U (2005) On the deduction of equations for the determination of anthropogenic influence for assessment of estuarine trophic status. Letter to the editor. Ecol Model 185(2–4):545–548. doi:10.1016/j.ecolmodel.2004.12.002

Berg P, Risgaard-Petersen N, Rysgaard S (1998) Interpretation of measured concentration profiles in sediment pore water. Limnol Oceanogr 437(7):1500–1510

Berner RA (1980) Early diagenesis: a theoretical approach. Princeton University Press, Princeton, NJ

Bijeljic B, Blunt MJ (2006) Pore-scale modeling and continuous time random walk analysis of dispersion in porous media. Water Resour Res 42:W01202. doi:10.1029/2005WR004578

Boudreau BP (1997) Diagenetic models and their implementation. Springer-Verlag, New York

Boudreau BP, Huettel M, Forster S, Jahnke RA, McLachlan A, Middelburg JJ, Nielsen P, Sansone F, Taghon G, Van Raaphorst W, Webster I, Weslawski JM, Wiberg P, Sundby B (2001) Permeable marine sediments: overturning an old paradigm. EOS 82(11):135–136

Bowen JL, Kroeger KD, Tomasky G, Pabich WJ, Cole ML, Carmichael RH, Valiela I (2007) A review of land–sea coupling by groundwater discharge of nitrogen to New England estuaries: Mechanisms and effects. Appl Geochem 22(1):175–191. doi:10.1016/j.apgeochem.2006.09.002

Brandes JA, Devol AH, Deutsch C (2007) New developments in the marine nitrogen cycle. Chem Rev 107(1):577–589. doi:10.1021/cr050377t

Burnett W, Bokuniewicz H, Huettel M, Moore W, Taniguchi M (2003) Groundwater and pore water inputs to the coastal zone. Biogeochemistry 66(1):3–33. doi:10.1023/B:BIOG.0000006066.21240.53

Burnett WC, Aggarwal PK, Aureli A, Bokuniewicz H, Cable JE, Charette MA, Kontar E, Krupa S, Kulkarni KM, Loveless A, Moore WS, Oberdorfer JA, Oliveira J, Ozyurt N, Povinec P, Privitera AMG, Rajar R, Ramessur RT, Scholten J, Stieglitz T, Taniguchi M, Turner JV (2006) Quantifying submarine groundwater discharge in the coastal zone via multiple methods. Sci Total Environ 367(2–3):498–543. doi:10.1016/j.scitotenv.2006.05.009 (Review)

Cable JE, Burnett WC, Chanton JP, Corbett DR, Cable PH (1997) Field evaluation of seepage meters in the coastal marine environment. Estuar Coast Shelf Sci 45(3):367–375. doi:10.1006/ecss.1996.0191

Cappuyns V, Swennen R, Devivier A (2004) Influence of ripening on pHstat leaching behaviour of heavy metals from dredged sediments. J Environ Monit 6(9):774–781. doi:10.1039/b406672c

Carleton JN (2002) Damköhler number distributions and constituent removal in treatment wetlands. Ecol Eng 19(4):233–248. doi:10.1016/S0925-8574(02)00094-0

DeSimone LA, Howes BL (1996) Denitrification and nitrogen transport in a coastal aquifer receiving wastewater discharge. Environ Sci Technol 30(4):1152–1162. doi:10.1021/es950366p

Dollhopf SL, Hyun J, Smith AC, Adams HJ, O'Brien S, Kostka JE (2005) Quantification of ammonia-oxidizing bacteria and factors controlling nitrification in salt marsh sediments. Appl Environ Microbiol 71(1):240–246. doi:10.1128/AEM.71.1.240-246.2005

Dullien F (1992) Porous media-fluid transport and pore structure. Academic Press Inc., San Diego, p 574

Falter L, Sansone FL (2000) Hydraylic control of pore water geochemistry within the oxic-suboxic zone of a permeable sediment. Limnol Oceanogr 45(3):550–557

Ferreira JG, Simas T, Nobre A, Silva MC, Shifferegger K, Lencart-Silva J (2003) Identification of sensitive areas and vulnerable zones in transitional and coastal Portuguese systems—application of the United States National Estuarine Eutrophication Assessment to the Minho, Lima, Douro, Ria de Aveiro, Mondego, Tagus, Sado, Mira, Ria Formosa and Guadiana systems. INAG and IMAR

Gran V, Pitkänen H (1999) Denitrification in estuarine sediments in the eastern Gulf of Finland, Baltic Sea. Hydrobiologia 393:107–115. doi:10.1023/A:1003530907516

Hamersley MR, Howes BL (2005) Evaluation of the N_2 flux approach for measuring sediment denitrification. Estuar Coast Shelf Sci 62(4):711–723. doi:10.1016/j.ecss.2004.10.008

Herbert RA (1999) Nitrogen cycling in coastal marine sediments. FEMS Microbiol Rev 23(5):563–590. doi:10.1016/S0168-6445(99)00022-4

Horn DP (2002) Beach groundwater dynamics. Geomorphology 48(1–3):121–146. doi:10.1016/S0169-555X(02)00178-2

Huettel M, Ziebis Z, Forster S, Luther GW (1998) Advective transport affecting metal and nutrient distributions and interfacial fluxes in permeable sediments. Geochimica and Cosmochimica Acta 62(4):613–631. doi:10.1016/S0016-7037(97)00371-2

Hulth S, Aller RC, Canfield DE, Dalsgaard T, Engstrom P, Gilbert F, Sundback K, Thamdrup B (2005) Nitrogen removal in marine sediments: recent findings and future research challenges. Mar Chem 94(1):125–145. doi:10.1016/j.marchem.2004.07.013

Jensen KM, Jensen MH, Kristensen E (1996) Nitrification and denitrification in Wadden Sea sediments (Konigshafen, Island of Sylt, Germany) as measured by nitrogen isotope pairing and isotope dilution. Aquat Microb Ecol 11(2):181–191. doi:10.3354/ame011181

Johannes RE (1980) The ecological significance of the submarine discharge of groundwater. Mar Ecol Prog Ser 3:365–373

Jones MN (1984) Nitrate reduction by shaking with cadmium: alternative to cadmium columns. Water Res 18(5):643–646. doi:10.1016/0043-1354(84)90215-X

Jørgensen SE (1994) Fundamentals of ecological modelling. In: Developments in environmental modelling, vol 19, second edn. Elsevier, Amsterdam, pp 628

Kim D-H, Matsuda O, Yamamoto T (1997) Nitrification, denitrification and nitrate reduction rates in the sediment of Hiroshima Bay, Japan. J Oceanogr 53:317–324

Kroeger KD, Charette MA (2008) Nitrogen biogeochemistry of submarine groundwater discharge. Limnol Oceanogr 53(3):1025–1039

Laima L, Brossard D, Sauriau P-G, Girard M, Richard P, Gouleau D, Joassard L (2002) The influence of long emersion on biota, ammonium fluxes and nitrification in intertidal sediments of Marennes-Ole′ ron Bay, France. Mar Environ Res 53(4):381–402. doi:10.1016/S0141-1136(01)00126-X

Lautz LK, Siegel DI (2006) Modeling surface and ground water mixing in the hyporheic zone using MODFLOW and MT3D. Adv Water Resour 29:1618–1633. doi:10.1016/j.advwatres.2005.12.003

Lee DR (1977) A device for measuring seepage flux in lakes and estuaries. Limnol Oceanogr 22(1):140–147

Leote C, Ibánhez JS, Rocha C (2008) Submarine groundwater discharge as a nitrogen source to the Ria Formosa studied with seepage meters. Biogeochemistry 88(2):185–194. doi:10.1007/s10533-008-9204-9

Luo Y, Qiao X, Song J, Christie P, Wong M (2003) Use of a multi-layer column device for study on leachability of nitrate in sludge-amended soils. Chemosphere 52(9):1483–1488. doi:10.1016/S0045-6535(03)00486-7

Mackenzie FT, Ver LM, Lerman A (2002) Century-scale nitrogen and phosphorus controls of the carbon cycle. Chem Geol 190(1–4):13–32. doi:10.1016/S0009-2541(02)00108-0

Moore SW (1999) The subterranean estuary: a reaction zone of ground water and sea water. Mar Chem 65(1–2):111–125. doi:10.1016/S0304-4203(99)00014-6

Nowicki BL, Portnoy J (1999) The role of sediment denitrification in reducing groundwater-derived nitrate inputs to Nauset Marsh estuary, Cape Cod, Massachusetts. Estuaries 22(2A):245–259. doi:10.1007/BF02692119

Nowicki BL, Van Keuren ERD, Kelly JR (1997) Nitrogen losses through sediment denitrification in Boston harbor and Massachusetts Bay. Estuaries 20(3):626–639. doi:10.1007/BF02692175

Pallud C, Meile C, Laverman AM, Abel J, Van Cappellen P (2007) The use of flow-through sediment reactors in biogeochemical kinetics: methodology and examples of applications. Mar Chem 106(1–2):256–271. doi:10.1016/j.marchem.2006.12.011

Rabouille C, Mackenzie FT, Ver LM (2001) Influence of the human perturbation on carbon, nitrogen, and oxygen biogeochemical cycles in the global coastal ocean. Geochimical et Cosmochimica Acta 65(21):3615–3641. doi:10.1016/S0016-7037(01)00760-8

Rapaglia JP, Bokuniewicz HJ (2009) The effect of groundwater advection on salinity in pore waters of permeable sediments. Limnol Oceanogr 54(2):630–643

Rivett MO, Buss SR, Morgan P, Smith JWN, Bemment CD (2008) Nitrate attenuation in groundwater: a review of biogeochemical controlling processes. Water Res 42(16):4215–4232. doi:10.1016/j.watres.2008.07.020

Robinson C, Li L, Barry DA (2007) Effect of tidal forcing on a subterranean estuary. Adv Water Resour 30(4):851–865. doi:10.1016/j.advwatres.2006.07.006

Rocha C (2008) Sandy sediments as active biogeochemical reactors: compound cycling in the fast lane. Aquat Microb Ecol 53:119–127. doi:10.3354/ame01221

Rocha C, Cabral AP (1998) The influence and dynamics of tidal action on porewater nitrate concentration in intertidal sediments of the Sado estuary. Estuaries 21(4A):635–645

Rocha C, Ibanhez J, Leote C (2009) Benthic nitrate biogeochemistry affected by tidal modulation of submarine groundwater discharge (SGD) through a sandy beach face, Ria Formosa, Southwestern Iberia. Mar Chem 115(1–2):43–58. doi:10.1016/j.marchem.2009.06.003

Roychoudhury AN (2001) Dispersion in unconsolidated aquatic sediments. Estuar Coast Shelf Sci 53(5):745–757. doi:10.1006/ecss.2001.0821

Rysgaard S, Christensen PB, Nielsen LP (1995) Seasonal variation in nitrification and denitrification in estuarine sediment colonized by benthic microalgae and bioturbating infauna. Mar Ecol Prog Ser 126:111–121. doi:10.3354/meps126111

Salles P (2001) Hydrodinamic controls on multiple tidal inlet persistence. PhD thesis, Massachusetts Institute of Technology/Woods Hole Oceanographic Institution

Schauser I, Hupfer M, Brüggemann R (2006) Sensitivity analysis with a phosphorus diagenetic model (SPIEL). Ecol Model 190(1–2):87–98. doi:10.1016/j.ecolmodel.2005.03.024

Seeberg-Elverfeldt J, Schluterl M, Fesekerl T, Kölling M (2005) Rhizon sampling of porewaters near the sediment-water interface of aquatic systems. Limnol Oceanogr Methods 3:361–371

Shaw RD, Prepas EE (1989) Anomalous, short-term influx of water into seepage meters. Limnol Oceanogr 34(7):1343–1351

Sheibley RB, Jackman AP, Duff JH, Triska FJ (2003) Numerical modeling of coupled nitrification-denitrification in sediment perfusion cores from the hyporheic zone of the Shingobee River, MN. Adv Water Resour 26(9):977–987. doi:10.1016/S0309-1708(03)00088-5

Slater JM, Capone DG (1987) Denitrification in aquifer soil and Nearshore marine sediments influenced by groundwater nitrate. Appl Environ Microbiol 53(6):1292–1297

Slomp CP, Van Cappellen P (2004) Nutrient inputs to the coastal ocean through submarine groundwater discharge: controls and potential impact. J Hydrol 295(1–4):64–86. doi:10.1016/j.jhydrol.2004.02.018

Soetaert K, Herman PMJ, Middelburg JJ (1996) A model of early diagenetic processes from shelf to abyssal depths. Geochim Cosmochim Acta 60(6):1019–1040. doi:10.1016/0016-7037(96)00013-0

Spiteri C, Slomp CP, Charette MA, Tuncay K, Meile C (2008) Flow and nutrient dynamics in a subterranean estuary (Waquoit Bay, MA, USA): field data and reactive transport modeling. Geochim Cosmochim Acta 72:3398–3412. doi:10.1016/j.gca.2008.04.027

Taniguchi M, Burnett WC, Dulaiova H, Kontar EA, Povinec PP, Moore WS (2006) Submarine groundwater discharge measured by seepage meters in Sicilian coastal waters. Cont Shelf Res 26:835–842. doi:10.1016/j.csr.2005.12.002

Ueda S, Go CU, Suzumura M, Sumi E (2003) Denitrification in a seashore sandy deposit influenced by groundwater discharge. Biogeochemistry 63(2):187–205

Ullman WJ, Aller RC (1982) Diffusion coefficients in nearshore marine sediments. Limnol Oceanogr 27:552–556

Usui T, Koike I, Ogura N (2001) N_2O production, nitrification and denitrification in an estuarine sediment. Coast Shelf Sci 52(7):769–781. doi:10.1006/ecss.2000.0765

Vanderborght J-P, Billen G (1975) Vertical distribution of nitrate concentration in interstitial water of marine sediments with nitrification and denitrification. Limnol Oceanogr 20:953–961

Vitousek PM, Mooney HA, Lubchenco J, Melillo JM (1997) Human domination of Earth's ecosystems. Science 277(5325):494–499. doi:10.1126/science.277.5325.494